ON OPTICAL QUANTIFICATION OF CAVITATION PROPERTIES

Stefan Borchert
Institute of General Electrical Engineering, University of Rostock, Germany

Willfried Kröger
Institute of General Electrical Engineering, University of Rostock, Germany

Stephan Höhne
Institute of General Electrical Engineering, University of Rostock, Germany

Nils Andreas Damaschke
Institute of General Electrical Engineering, University of Rostock, Germany

Zhiliang Zhou
Institute for Graphical Data Processing, Fraunhofer Institute, Germany

SUMMARY

This paper investigates quantitative cavitation characterization. In this context we propose shadow imaging to determine cavitation thickness and tip vortex volume. We propose a laser adjustment for absolute calibration and address cavitation extent by means of image processing.

We present advantages and disadvantages of automatic processing with regard to our proposed techniques. Our main focus is on the novel cavitation thickness and tip vortex occurrence processing. Due to turbulent fluctuations all used techniques provide statistical results. The accuracy of single measurements mainly depends on camera resolution, aberrations in the optical path, illumination and optical access.

INTRODUCTION

In the framework of a joint research project between Hamburg Ship Model Basin (HSVA), Potsdam Model Basin (SVA), Technical University of Hamburg Harburg (TU-HH) and University of Rostock (URO), supported by the Federal Ministry of Economics and Technology (BMWI), quantitative measurements for determination of water quality and its influence on cavitation processes are performed. The goal of the project is a reliable prognosis of cavitation on ship propellers based on experiments in cavitation tunnels.

We propose image processing techniques to quantify cavitation properties like cavitation thickness, cavitation extent and tip vortex volume. Conventionally, experts at the model basins use their experience to accurately describe cavitation by means of drawings. In addition, photos and high speed videos are provided to customers. However, the information derived from this data is mostly limited to the cavitation extent and the area of the tip vortex. To better describe the cavitation thickness, laser based techniques have been described in [1] and in [2]. Here, laser glares are employed to measure the cavitation thickness. As this is only a pointwise measurement, a grid needs to be traversed.

In this paper we propose a shadow imaging method to measure cavitation thickness. Since introducing a calibration target into the cavitation tunnel is impractical, we propose a calibration based on a laser beam and on foil markings. Stroboscopic lighting and minimum camera exposure time eliminate motion blur. In addition to the cavitation thickness, we further investigate cavitation extent and tip vortex volume.

CAVITATION TUNNELS

In [3] cavitation is defined as ”the process of nucleation in a liquid when the pressure falls below the vapor pressure”. Such vapor bubbles collapse and cause microjets. ”When this collapse occurs close to a solid surface, these intense disturbances generate highly localized and transient surface stresses” [3]. Hence cavitation can damage propellers and rudders.

The main purpose of model basins is to test new propeller or ship designs with regard to their cavitation behavior. The model basin has to accurately predict the cavitation behavior and consequently the safe ship speed. The margin for error is small as small deviations between promised and actual speed can yield large delays on longer ship voyages.

We performed measurements at multiple cavitation channels. These are the K15A at the SVA, the K22 and HYKAT at the HSVA, the K21 at the University of Rostock and the K27 at the Technical University of Berlin. The tunnels vary in size, water volume and optical access. An overview of key properties is provided in Table 1. Since shadow imaging relies on capturing transmitted light, two face to face windows are preferred. If such windows are unavailable, we have to rely on non-point i.e. diffuse reflection.

An example of such an experimental setup is shown in Fig. 1. While the focus of the paper is on cavitation thickness, the cavitation extent was captured as well. Its processing is straightforward

Proceedings of the Eighth International Symposium on Cavitation (CAV 2012)
Edited by Claus-Dieter OHL, Evert KLASEBOER, Siew Wan OHL, Shi Wei GONG and Boo Cheong KHOO.

ISBN: 978-981-07-2826-7 :: doi:10.3850/978-981-07-2826-7_174

Table 1. Cavitation tunnel properties

cavitation tunnel	location	cross-section area	water volume	height
K15A	SVA	600 x 600mm^2 850 x 850mm^2	38m^3	7m
K21	URO	300 x 300mm^2	3.4m^3	1.8m
K22	HSVA	600 x 600mm^2	32m^3	8m
K27	TUB	600 x 600mm^2	260m^3	8.4m
HYKAT	HSVA	2800 x 1600mm^2	1500m^3	11m

(a) Shadow imaging camera.

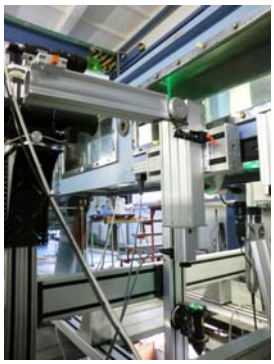

(b) Cavitation extent camera.

Figure 1. Experimental setup for 2D foil at K15A.

and luminance based.

SHADOW IMAGING

Shadow imaging is a standard technique used for characterization of two phase flows. Beside a number of applications for droplet sizing, imaging of bubbles is presented by various authors (e.g. [4–6]). In principle, structures are captured in transmitted light. Consequently, they appear as dark shadows on a bright background. The advantage of shadow imaging is the independence of glare spots due to reflection and refraction. Well designed illuminates enables accurate size measurements.

For a cavitating 2D foil, cavitation occurs along the whole length of the foil. To measure at specific positions we have to rely on the sharpness. A small depth of focus and a large number of frames are required to capture reliable statistics. With the camera set up parallel to the foil, the upper half of the aperture enables an observation from above. Within limits it is possible to look above out-of-focus cavitation.

In Fig. 2 we show the difference between a shadow image for the foil without and with cavitation. The depth of focus is small and only a very limited range shows sharp lines (either on the foil or caused by the cavitation).

Stroboscopic light sources prevent motion blur since it is possible to achieve high luminance with very small exposure times. For imaging we use up to four standard CCD cameras and

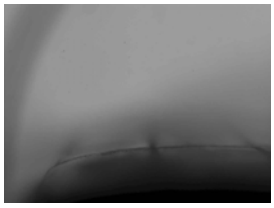

(a) 2D foil without cavitation.

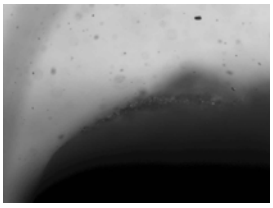

(b) 2D foil with cavitation.

Figure 2. Shadow images for 2D foil.

two high speed cameras with different viewing angles. To minimize aberrations a viewing angle perpendicular to the observation window is preferred. For the experiments a number of devices are used at different operating points of the cavitation tunnel.

Measurements include a 2D foil, a 3D foil, two propellers in homogeneous inflow and one propeller with model ship. For the 2D foil we only consider cavitation thickness and extent. For the remaining devices we also consider tip vortex volume.

INVESTIGATIONS

Absolute Calibration

An absolute calibration is required to get a conversion factor between units. In our case we need to relate a number of pixels to a physical distance [mm]. For that purpose we use a small laser module. The laser beam is targeted at the desired depth of focus on the 2D foil. We then adjust the focal plane of the object lens to the laser.

We use a traverse system to move the laser beam within the measurement area. The measurement area is approximately the front 4 cm of the 2D foil. We then use a step size of 2 mm. At each laser beam position we capture multiple frames. The visibility of the laser beam is only high when particles are passing through. The longer we record each position the more particles pass through the beam. Consequently, averaging all frames for one laser position yields a clear luminance maximum for the beam.

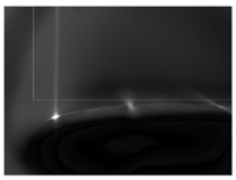

(a) Average laser position.

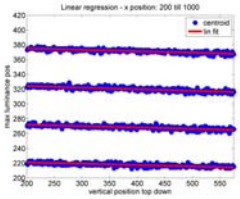

(b) Several laser positions.

Figure 3. Average of one laser position with ROI and linear regression of multiple laser positions.

Fig. 3 shows an averaged frame for one laser position. We use a region of interest (ROI) to capture only the laser beam. For each top down ROI line we find the maximum luminance. A corresponding linear regression for each laser beam position is shown in Fig. 3. If the mean distance between neighboring laser

beams stays constant, i.e. the standard deviation is small, we can calculate an accurate conversion factor. The factor in our example is about 25 pixels per mm. Hence, the upper bound for accuracy is 40 µm/pixel.

Shadow image processing

Every cavitation tunnel setting has an impact on the amount of cavitation. Relevant parameters are tunnel speed, tunnel vapor pressure, blade angle and bubble concentration. Even a single measuring point behaves intermittently. To account for the fluctuation we capture about 4000 frames for each measuring point. In addition, not all frames contain a sharp in-focus cavitation edge due to occlusion by out-of-focus cavitation.

Identifying the foil edge is possible with only few frames. Each frame is processed with a sensitive canny edge detector. Outliers are eliminated by taking the maximum occurrence over 200 frames. The smaller the depth of focus the better. A large depth of focus can induce artifacts by finding two distinct foil edges. On average however the foil edge is still valid.

To identify the cavitation edge, each frame is processed with a stricter canny edge detector. The strictness, i.e. the canny parameters, are adaptively chosen and are highly dependent on lighting conditions. To exclude vapor bubbles, which can also be in focus, we limit processing to the lowest edge. Hence, the foil is assumed to be uniformly dark. This assumption does not hold for all lighting conditions, varying with the blade angle.

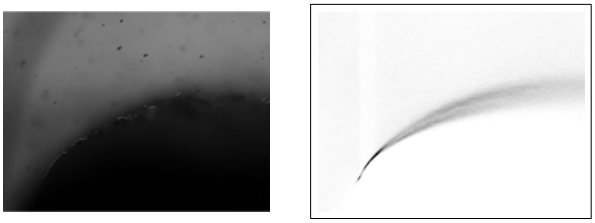

(a) Example edge. (b) Accumulated edges.

Figure 4. Example for measurement - single frame and resulting edges over all frames.

A frame where the assumption is valid is displayed in Fig. 4. The found cavitation edge is visualized in white. We observe areas where the lowest edge is found on bubbles above the cavitation. In these areas no in-focus cavitation is visible. A result of accumulated edges is shown in Fig. 4 as well. The brightness is a measure for occurrence of edges. To account for the spread, i.e. the intermittent cavitation behavior we opt for 3 distinct cavitation edges.

Lower cavitation edge - Below this edge no vapor-liquid surface was observed. Therefore, the line represents the minimum stable thickness of the cavitation sheet. As can be seen in Fig. 4 b the lower edge is relatively sharp and stable.
Mean cavitation edge - Between both borders an average cavitation extension can be defined. The line is calculated as a mean from detected edges, more precisely it represents the edge which can be observed most frequently.
Upper cavitation edge - Over the cavitation sheet bubbles from the inflow, bubbles separated from the vapor volume and vapor ligaments occur. The upper cluster of detected edges in Fig. 4 b suggests a sharp transition from structures still connected to the dark cavitation sheet and free bubbles. The transition is can be labeled upper cavitation edge

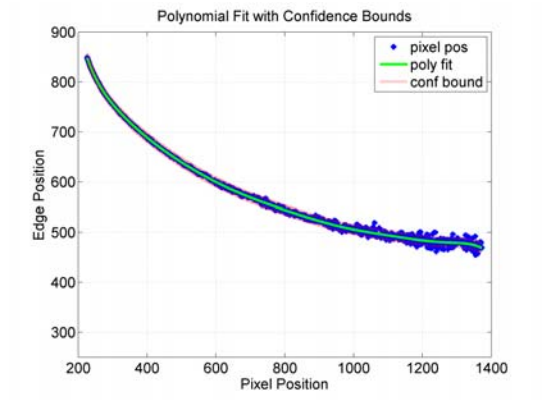

(a) Example polynomial fit.

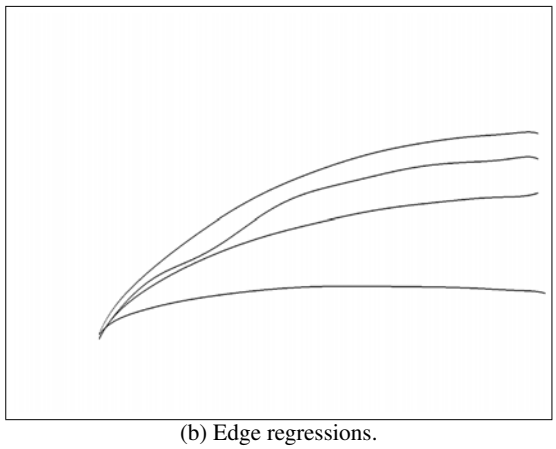

(b) Edge regressions.

Figure 5. Example for regression lines. a) polynomial fit for highest occurrence and b) resulting regressions for foil and three cavitation edges.

For regression we found a polynomial fit to provide good results. Fig. 5 shows an example fit for the lower cavitation edge. In addition, all four polynomial fits are shown. It should be noted that there is a small slackness to the 2D foil. Hence, it moves by a small margin due to pressure and the cavitation edges can fall below the foil edge.

We have to account for two special cases. First, if only very little cavitation is present (which is a desired measurement point) and second if the blade angle is 10 degree (also a desired measurement point). In both cases the assumption of the lowest edge being a cavitation edge does not hold. All detected edges are taken into account and the lowest detected edge is subtracted from the accumulated edges.

Finally, we use the conversion factor from the calibration

to provide physical distances. The resulting edges are stored as ASCII text files, which are then used by the TUHH as reference for their cavitation simulations.

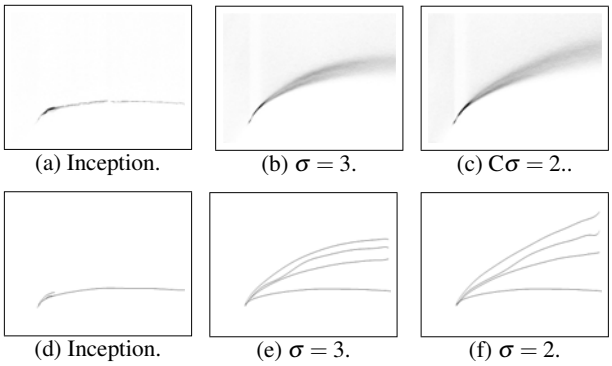

(a) Inception. (b) $\sigma = 3$. (c) C$\sigma = 2$.. (d) Inception. (e) $\sigma = 3$. (f) $\sigma = 2$.

Figure 6. Example hysteresis. a)-c) sum of edges and d)-e) resulting regression edges.

An example hysteresis for the 2D foil is illustrated in Fig. 6. Parameters that remain constant are a 15 degree angle of attack, a flow velocity of 4.5 m/s and saturated oxygen at approximately 60%. The cavitation number σ varies with the pressure.

The shown examples constitute the following measurement points:

1. a+d **Cavitation inception** Begin sheet cavitation. Sheet only occasionally present at measurement plane.
2. b+e **Cavitation number** $\sigma = 3$ Widespread cavitation.
3. c+f **Cavitation number** $\sigma = 2$ Maximum investigated cavitation. More volatile than $\sigma = 3$.

Cavitation extent

The cavitation extent is captured with stroboscopic illumination as shown in Fig. 7. Since the measurements are performed synchronously with the cavitation thickness measurements the lighting is not ideal for either. In addition, intermittent cavitation poses a challenge for processing. Fig. 8 illustrates the problem.

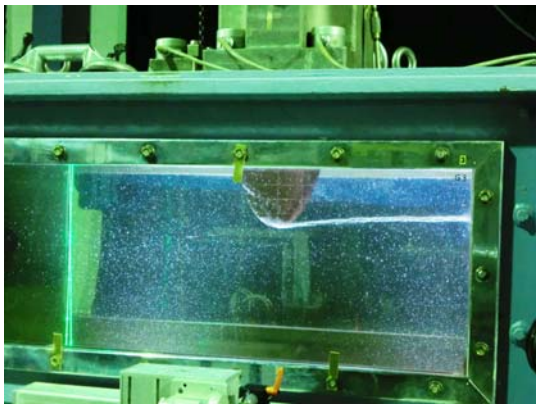

Figure 7. Lighting conditions for 3D foil.

The foil markings with their known physical distance provide the absolute calibration. Instead of average laser beams we detect the markings and compute their image distance. The segmentation of cavitation extent suffers from bad lighting conditions and is highly dependent on the dynamic threshold. We use the threshold to perform a binarization after background subtraction.

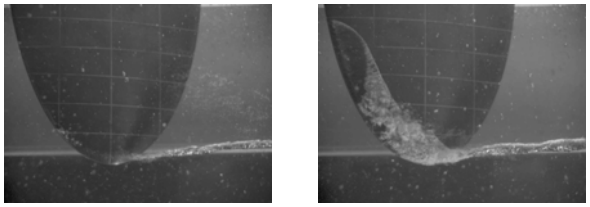

Figure 8. Cavitation spread on 3D foil - identical measuring point.

Due to either slight deformation of the tunnel windows or slight dislocation of the 3D foil a simple background subtraction is difficult. Non-cavitating measurement points are insufficient and we need to extract a background representation from the cavitation sequence itself. We take the first 200 (out of 3500) frames and for each position the darkest pixel value is taken. Since the contrast is low, the segmentation that can be generated for each frame suffers. The sum of these segmentations provides an estimate for cavitation extent occurrence. However, the process is highly volatile and the confidence level by comparison low. An example estimate is shown in Fig. 9.

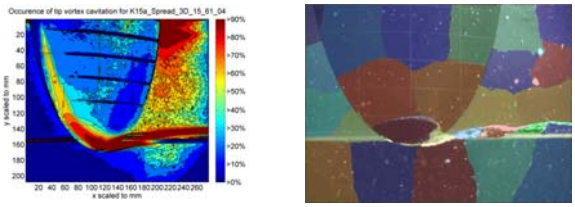

(a) Cavitation extent. (b) Normalized cut clustering.

Figure 9. Segmentation results for 3D foil.

The processing of the tip vortex was done in cooperation with the Institute for Graphical Data Processing, Fraunhofer Institute. A spatial segmentation based on weighting factors is performed. The factors are edge information, local neighborhood and luminance. The NCut algorithm [7] provides a segmentation result which can then be analyzed across frames. Fig. 9 shows an example for NCut clustering.

Tip vortex

There are multiple problems when applying our cavitation thickness measurements to the propeller case. First and foremost, the cavitation tunnels have restricted optical access. The access is further limited by the concurrent phase Doppler measurements. To acquire an optical axis parallel to the propeller surface, a skewed viewing angle is required. Due to optical aberrations, especially astigmatism, a sufficiently sharp depth-of-focus

is not possible without optical coupling.

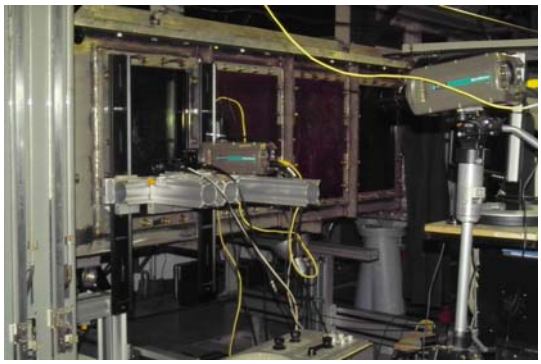

Figure 10. Experimental setup for propeller at K15A.

To account for the challenging optical conditions, the focus shifted to the tip vortex processing as key measure. For that purpose two identical cameras (with identical object lenses) are aligned to provide two views. The first camera is set up to a straight viewing angle with least aberrations. The second camera is horizontally displaced by a small margin and provides a better estimate of the physical extension of the tip vortex. The margin is kept small to limit the skew in viewing angle and hence the astigmatism.

Nevertheless, the sharpness suffers from the skewed viewing angle. A third camera is set up to capture the tip vortex on the propeller blade itself, i.e. provides an estimate of the maximum cavitation thickness. The camera setup, including a fourth high speed camera, is shown in Fig. 10.

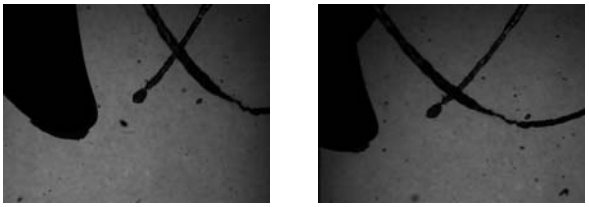

(a) Stereo 1. (b) Stereo 2.

Figure 11. Example tip vortex frames for both stereo cameras.

The tip vortex images are captured with transmitted light, providing good contrast. Two example recordings are shown in Fig. 11. The dark areas are comprised of the propeller blades, solid particles, bubbles and cavitation (vapor) areas. With dynamic thresholding it is possible to provide a binary representation of the images. The binary images which correspond to the frames shown in Fig. 11 are provided in Fig. 12.

Each binary frames represents a momentary state of the tip vortex. The sum of these stats provide a statistical measure for cavitation occurrence. The number of captured frames determines the confidence level, but is limited by measurement time, storage space, storage speed and frame rate. While the cavitation thickness sequences provide only partial information for many frames, every stereo frame provides complete information. Consequently, we captured less than 2000 frames for each stereo camera.

(a) Stereo 1. (b) Stereo 2.

Figure 12. Example binarized tip vortex frames for both stereo cameras.

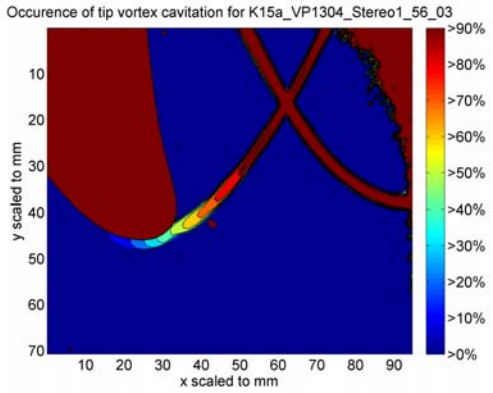

(a) Stereo 1.

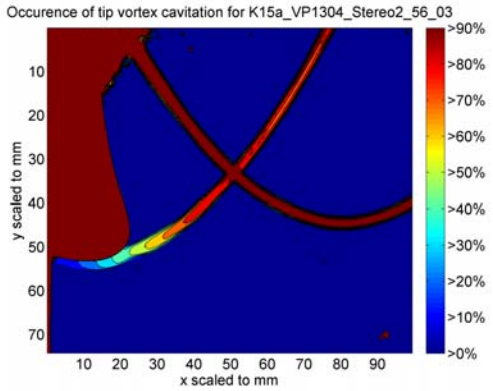

(b) Stereo 2.

Figure 13. Tip vortex occurrence for both stereo cameras.

Fig. 13 shows the tip vortex occurrence for the two examples. The occurrence is divided into 10 percent steps. It should be noted that the same dynamic threshold was used for both sequences. As a consequence, the blur induced by the skewed viewing angle from stereo camera 2 causes an offset of approximately 10 percent. In addition, both cameras show artifacts from either tunnel window, object lens or camera chip staining.

Table 2. Accuracy factors for cavitation thickness and tip vortex.

foil/ propeller	**depth-of-focus**	**lighting**	**viewing angle**	**distance**
2D foil	critical	critical	low	low
3D foil	critical	critical	critical	critical
propeller	low	critical	low / high	high

Accuracy

The processing is performed with pixel accuracy. There are however numerous factors affecting the overall accuracy:

1. **Cavitation process:** Highly intermittent cavitation behavior.
2. **Optical aberrations:** Affected by f.i. viewing angle, distance, camera and object lens.
3. **Depth-of-focus:** Size of measurement plane.
4. **Confidence level:** Number of captured frames.

Both cavitation process and confidence level are mostly fixed parameters, assuming the measurement time is limited. The importance of the remaining factors (or their causes) differs for each measurement object. Table 2 provides an overview of the relative factor importance.

In the following we analyze the depth-of-focus for the 2D foil. First, the depth-of-focus depends on camera properties like resolution and physical pixel size on chip. These parameters determine the circle of confusion c. Second, the object lens with its focal length f and f-number N is crucial. Finally, the distance between camera and measurement plane s as well as the medium in between plays a role.

The depth-of-focus or depth-of-field DOF can f.i. be calculated as follows:

$$DOF = \frac{2Ncf^2s^2}{f^4 - N^2c^2s}. \quad (1)$$

The corresponding values for the experiment are $c \approx 0.007mm$, $f = 60mm$, $N = 2.8$ and $s \approx 330mm$ and result in $DOF \approx 1.2mm$. Instead of an infinitely thin measurement plane we actually observe a volume. Especially for the 2D foil without cavitation the DOF can result in 2 detected edges (lower and upper limit of DOF) instead of one. The problem intensifies for the 3D foil as s is much larger, the viewing angle is skewed and lighting conditions are worse. However, since cavitation is by no means stationary the intermittent process behavior obscures measurement inaccuracies.

By contrast, the propeller tip vortex measurements are less restrictive in their optical requirements. The accuracy mainly depends on the distance s and the camera resolution. The optical setup at the K15A accounts for 70 µm.

CONCLUSIONS

In this paper we show a working cavitation thickness quantification. While it is possible to increase accuracy by means of camera resolution and object lens properties, the cavitation process itself is highly non-stationary. We account for this non-stationarity by providing three cavitation thicknesses.

We proceed to further measurements employing a 3D foil and different propellers. Due to restricted optical access, a moving system and a 3D surface, processing is more challenging. In addition to cavitation thickness and extent, there is also the tip vortex to evaluate. We propose a segmentation based approach to the tip vortex. The difficulty of the segmentation depends mainly on the lighting conditions. For the presented propeller case, an accurate tip vortex occurrence can be determined.

In the course of the project numerous data points have been accumulated. In total, 700 measurement points have been recorded.

ACKNOWLEDGMENTS

The authors would like to thank the Federal Ministry of Economics and Technology (BMWI) for supporting the project KonKav I. Further thanks go to the project partners SVA, HSVA and to Chair of Fluid Mechanics at University of Rostock to provide the cavitation tunnels, to the chair of Fluid Dynamics and Ship Theory at Hamburg University of Technology and to Dr. Weiterdorf.

REFERENCES

[1] Kodama, Y., Y., T., and Kakugawa, A., 1991. "Measurements of cavity thickness on a full scale ship using lasers ad a tv camera". In Eighteenth Symposium on Naval Hydrodynamics, pp. 319–330.

[2] Stinzing, H., 1989. *Bestimmung der Kavitationsschichtdicken an rotierenden Propellerflügeln mittels eines laseroptischen Verfahrens*. Bericht. Forschungszentrum des Dt. Schiffbaus.

[3] Brennen, C., 1995. *Cavitation and bubble dynamics*. Oxford University Press.

[4] Dehaeck, S., 2007. "Development of glare point, shadow and interferometric planar techniques for gas bubble sizing". Phd, University of Ghent.

[5] Bröder, D., and Sommerfeld, M., 2007. "Planar shadow image velocimetry for the analysis of the hydrodynamics in bubbly flows". *Measurement Science and Technology,* ***18***(8), p. 2513.

[6] Honkanen, M., 2006. *Direct Optical Measurement of Fluid Dynamics and Dispersed Phase Morphology in Multiphase Flows*. Tampere University of Technology.

[7] Shi, J., and Malik, J., 2000. "Normalized cuts and image segmentation". *Pattern Analysis and Machine Intelligence, IEEE Transactions on,* ***22***(8), aug, pp. 888 –905.